G. B. WALLIS
Associate Professor,
Thayer School of Engineering,
Dartmouth College,
Hanover, N. H. Assoc. Mem. ASME;
Also, Creare, Inc.,
Hanover, N. H.

Annular Two-Phase Flow

Part 1: A Simple Theory

A simple theory for annular two-phase flow is developed in terms of equations for the interfacial and wall shear stresses. Expressions for the pressure drop and void fraction are derived. Criteria for the minimum pressure drop, zero wall shear, and flow regime transition in vertical flow are given. The results are compared with numerous data and alternative theories from the literature.

Introduction

Up to now there have been two approaches to annular flow which were generally available to the engineer. The first was the use of some very crude, but easy-to-use, correlations such as Martinelli's or the various versions of homogeneous flow theory. The second was the piecing together of a calculation procedure from analyses or correlations of parts of the flow which have been described in some detail by research workers.

The disadvantage of both techniques is that neither provides a conceptual framework within which the whole picture can be developed with appropriate sophistication. Sweeping correlations suffer from their basic inflexibility, a lack of relationship to meaningful physical phenomena, and the awkwardness of adapting them to take account of secondary effects. The synthesizing of many bits and pieces of scientific work, on the other hand, is arduous and quite often becomes a research topic in itself. The nonspecialist just does not have the time to study the ways in which the theories of many different authors are related.

The objective of the first of these two papers is to present a theory of annular flow which is sufficiently simple to be useful and, at the same time, is based on the major physical phenomena which occur. Comparison is made with a wide variety of data and with other theories from the literature which can be rearranged into a similar form. Because the parameters in the theory are physically motivated, they are readily related to more complex analyses by means of correction factors. This is done in the second paper [18][1] in which several more specialized investigations are interpreted in terms of the overall conceptual structure. Thus the simple theory is like the apex of a pyramid which stands on a framework composed of more thorough scientific studies. Hopefully, additional information can be inserted into this pyramid at suitable levels as it is developed. Thus it is easier to grasp the significance of new information.

[1] Numbers in brackets designate References at end of paper.

Contributed by the Fluids Engineering Division and presented at the Applied Mechanics and Fluids Engineering Conference, Evanston, Ill., June 16–18, 1969, of The American Society of Mechanical Engineers. Manuscript received at ASME Headquarters, March 20, 1969. Paper No. 69-FE-45.

Development of a Simple Theory for Vertical Annular Flow

Qualitative Aspects. Vertical annular flow resembles the sketch shown in Fig. 1. Gas, which may contain suspended droplets, flows in a central core, while liquid flows in an annular film. The interface between the gas and the liquid usually appears wavy, and much of the interfacial shear stress, τ_i, is due to form drag on these waves. If the film has a mean thickness, δ, the fraction of the cross section which it occupies is

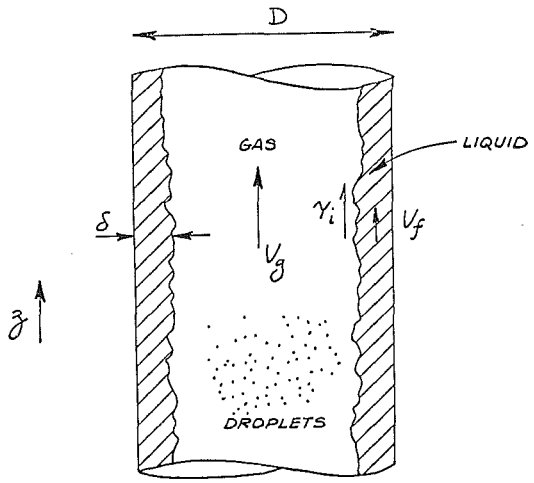

Fig. 1 Sketch of vertical annular flow

Nomenclature

D = pipe diameter
f = friction factor
F^1 = Levy parameter [see equation (36)]
g = acceleration due to gravity
G = mass flux
j = volumetric flux
k_s = sand roughness
p = pressure
Q = volumetric flow rate
R = Levy parameter [see equation (36)]
V = velocity
z = distance down pipe
α = void fraction
δ = film thickness
μ = viscosity
ρ = density
τ = shear stress
ϕ_g = Martinelli parameter

Subscripts

c = core
f = liquid
g = gas
i = interface
w = wall

Dimensionless Groups

j_f^* = turbulent liquid flux, equation (25)
j_f^{1*} = laminar liquid flux, equation (26)
j_g^* = turbulent gas flux, equation (24)
N_f = liquid viscosity, equation (31)
ΔP^* = pressure drop, equation (23)
Re_f = liquid Reynolds number, equation (30)

Abbreviations

CISE = Centro informazioni studi esperienze, Segrate, Milan, Italy
UKAEA = United Kingdom Atomic Energy Authority

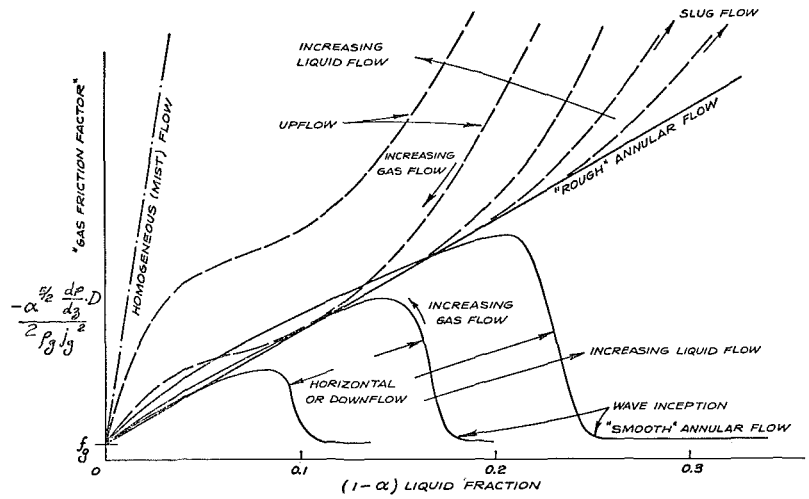

Fig. 2 Qualitative aspects of pressure-drop characteristics of various flow regimes

$$(1 - \alpha) = 1 - \frac{(D - 2\delta)^2}{D^2} = \frac{4\delta}{D}\left[1 - \frac{\delta}{D}\right] \tag{1}$$

The mean diameter of the gas stream is

$$D\sqrt{\alpha} = D - 2\delta \tag{2}$$

Suppose that one treats the gas stream as flowing in a "rough" pipe with walls composed of the interface. By analogy with single-phase flow, we define a fraction factor, f_i, by the relationship

$$f_i = \frac{\tau_i}{1/2\rho_g V_g^2} \tag{3}$$

The interface has been assumed to be stationary since, in most cases, $V_g \gg V_f$.

Performing a force balance for the central core of the flow, we find, in the absence of compressibility effects and area change

$$\frac{dp}{dz} + \rho_g g + \frac{4\tau_i}{D\sqrt{\alpha}} = 0 \tag{4}$$

whence, from equation (3)

$$\frac{-dp}{dz} - \rho_g g = f_i 1/2\rho_g V_g^2 \cdot \frac{4}{D\sqrt{\alpha}} \tag{5}$$

In most cases, $dp/dz \gg \rho_g g$, and the friction factor can be expressed as

$$f_i = \frac{-dp/dz\, D\sqrt{\alpha}}{2\rho_g V_g^2} \tag{6}$$

Usually one does not know V_g directly, but only the gas volumetric flow rate Q_g and the "void fraction" α. The mean volumetric gas flux, j_g, is defined to be

$$j_g = \frac{4Q_g}{\pi D^2} \tag{7}$$

The mean gas velocity then follows as

$$V_g = \frac{j_g}{\alpha} \tag{8}$$

and equation (6) becomes

$$f_i = \frac{-dp/dz \cdot D \cdot \alpha^{5/2}}{2\rho_g j_g^2} \tag{9}$$

Fig. 2 shows a plot of the interfacial friction factor versus liquid fraction for both upflow, horizontal flow, and downflow, and serves to indicate the various regimes of flow.

In horizontal or downflow at low gas velocities, the liquid film is smooth and the friction factor is approximately the smooth pipe value. Above a critical gas velocity for wave inception, the friction factor rises rapidly to a maximum after which it tends to follow the line marked "rough annular flow." The onset of waves is dependent on the surface tension, among other variables, and has not been successfully rationalized yet. At higher gas velocities, the tops of the waves are sheared off to form entrained droplets and the density of the core increases. This leads to an increase in the friction factor, defined by equation (9), in about the ratio ρ_c/ρ_g, where ρ_c is now the average homogeneous density of the core.

At very high flow rates of both phases, almost all of the liquid flow is entrained, and the pressure drop is given by "homogeneous" flow theory as

$$\frac{-dp}{dz} = f \cdot j_g[G_g + G_f] \cdot \frac{2}{D} \tag{10}$$

The symbol G represents the mass flow rate divided by the total pipe area. Equation (10) can be rearranged to give

$$\frac{-dp}{dz} = f\rho_g j_g^2 \left[1 + \frac{G_f}{G_g}\right] \frac{2}{D} \tag{11}$$

In homogeneous flow the liquid fraction is

$$(1 - \alpha) = \frac{Q_f}{Q_f + Q_g} \tag{12}$$

Usually the volumetric flow rate of the gas is much greater than the liquid flow rate, and equation (12) can be approximated by

$$(1 - \alpha) \approx \frac{Q_f}{Q_g} = \frac{\rho_g}{\rho_f} \cdot \frac{G_f}{G_g} \tag{13}$$

Using equation (13) in equation (11), we find that

$$\frac{-dp}{dz} = f\rho_g j_g^2 \left[1 + \frac{\rho_f}{\rho_g}(1 - \alpha)\right] \cdot \frac{2}{D} \tag{14}$$

If the friction factor in homogeneous flow is relatively unchanged from the value for gas alone, f_g, [as it usually is] we can use equation (14) to show that

$$\frac{-dp/dz \cdot D \cdot \alpha^{5/2}}{2\rho_g j_g^2} = f_g \left[1 + \frac{\rho_f}{\rho_g}(1 - \alpha)\right] \cdot \alpha^{5/2} \tag{15}$$

For air and water at atmospheric pressure $\rho_f/\rho_g \approx 800$ and for homogeneous flow, the value of equation (15) increases very rapidly as a fraction of $(1 - \alpha)$, as shown in Fig. 2. The curves tend to move toward the homogeneous flow line as the liquid rate is increased and the percent entrained goes up accordingly.

In vertical flow, the interfacial shear has to support the film

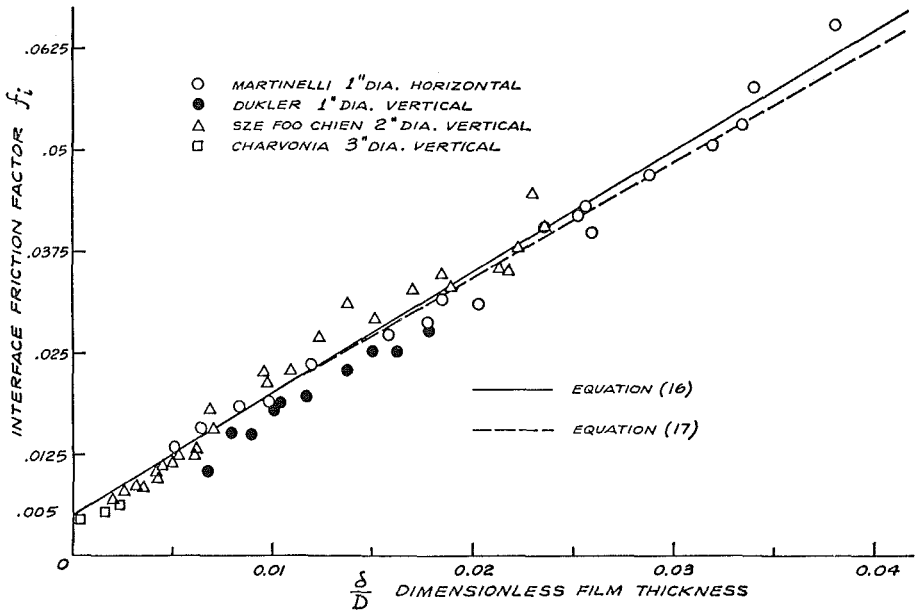

Fig. 3 Comparison between equations (16) and (17) and air-water data

against gravity. Furthermore, any slugs of liquid or entrained droplets add a gravitational component to the core pressure drop. Thus, at low gas rates in the slug flow region, the "friction factor" defined by equation (9) increases well above the annular flow value. At lower liquid rates this is usually at values of liquid fraction above about 0.2. At high liquid rates, the transition between slug flow and annular mist flow becomes obscure and there is a general motion toward the homogeneous flow line.

Interfacial Shear Stress. The interfacial shear stress has been discussed by many authors and is usually represented in a rather complicated way. The key to the present analysis is a simple plot of the interfacial friction factor versus the dimensionless film thickness, as shown in Fig. 3. The points cluster pretty well around a line with equation

$$f_i = 0.005\left[1 + 300\,\frac{\delta}{D}\right] \tag{16}$$

In view of equation (1), this is approximately the same as

$$f_i = 0.005[1 + 75(1 - \alpha)] \tag{17}$$

We note at this point that the rough pipe correlations of Nikuradse [3] and Moody [4] can be approximated by the equation

$$f \approx 0.005\left[1 + 75\,\frac{k_s}{D}\right] \tag{18}$$

over the range $0.001 < k_s/D < 0.03$, where k_s is the grain size of a "sand roughness." Equation (16), therefore, shows that a wavy annular film is about equivalent to a sand roughness of four times the film thickness.

Using equations (16), (8), and (3) in equation (4), we obtain

$$-\left(\frac{dp}{dz} + \rho_g g\right) = 10^{-2}\cdot\frac{\rho_g j_g^{\,2}}{D}\cdot\frac{[1 + 75(1 - \alpha)]}{\alpha^{5/2}} \tag{19}$$

Another way to look at equation (19) (apart from the small gravitational term) is to say that the pressure drop is increased above the value for the gas alone in the pipe by a factor, ϕ_g^2, which was originally introduced by Martinelli [5]. Taking the friction factor for the gas alone as 0.005, we readily obtain

$$\phi_g = \frac{[1 + 75(1 - \alpha)]^{1/2}}{\alpha^{5/2}} \tag{20}$$

Fig. 4 shows that equation (20) is intermediate between several expressions which are due to other authors.

Turner [6], among others, has shown that it is reasonable to assume that the wall shear stress is the same as it would be if the liquid film were part of a liquid stream filling the whole pipe. In turbulent flow, with a wall friction factor of 0.005, a force balance on the whole flow gives

$$-\left[\frac{dp}{dz} + \rho_g g\right] = (1 - \alpha)(\rho_f - \rho_g)g + 10^{-2}\,\frac{\rho_f j_f |j_f|}{D(1 - \alpha)^2} \tag{21}$$

In the case of laminar flow, it is more accurate to solve the differential equations across the film to get the result

$$-\left[\frac{dp}{dz} + \rho_g g\right] = 32\,\frac{j_f \mu_f}{D^2(1 - \alpha)^2} + \left[1 - \frac{2\alpha^2 \ln \alpha}{(1 - \alpha)^2} - \frac{2\alpha}{1 - \alpha}\right] g(\rho_f - \rho_g) \tag{22}$$

The final square bracket in equation (22) can be closely approximated [6] over the range $D < (1 - \alpha) < 0.2$ by the value $(0.684)(1 - \alpha)$.

It is convenient at this point to define dimensionless forms of the pressure drop and flow rates as follows

$$\Delta P^* = \frac{-[dp/dz + \rho_g g]}{g(\rho_f - \rho_g)} \tag{23}$$

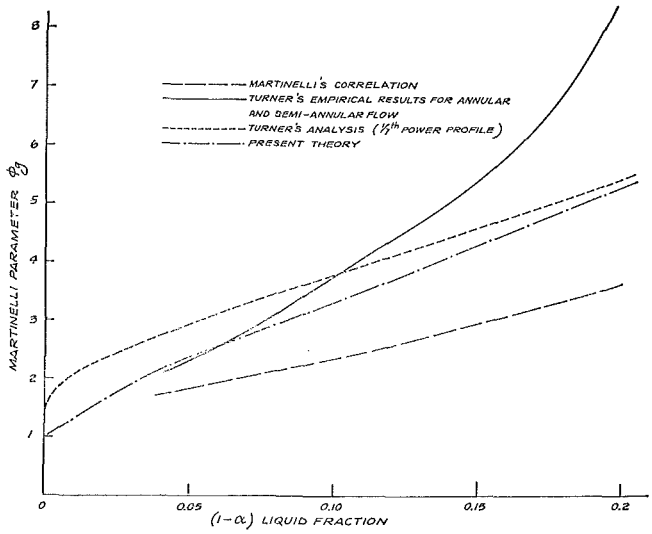

Fig. 4 Expression of present theory in terms of Martinelli's parameter ϕ_g

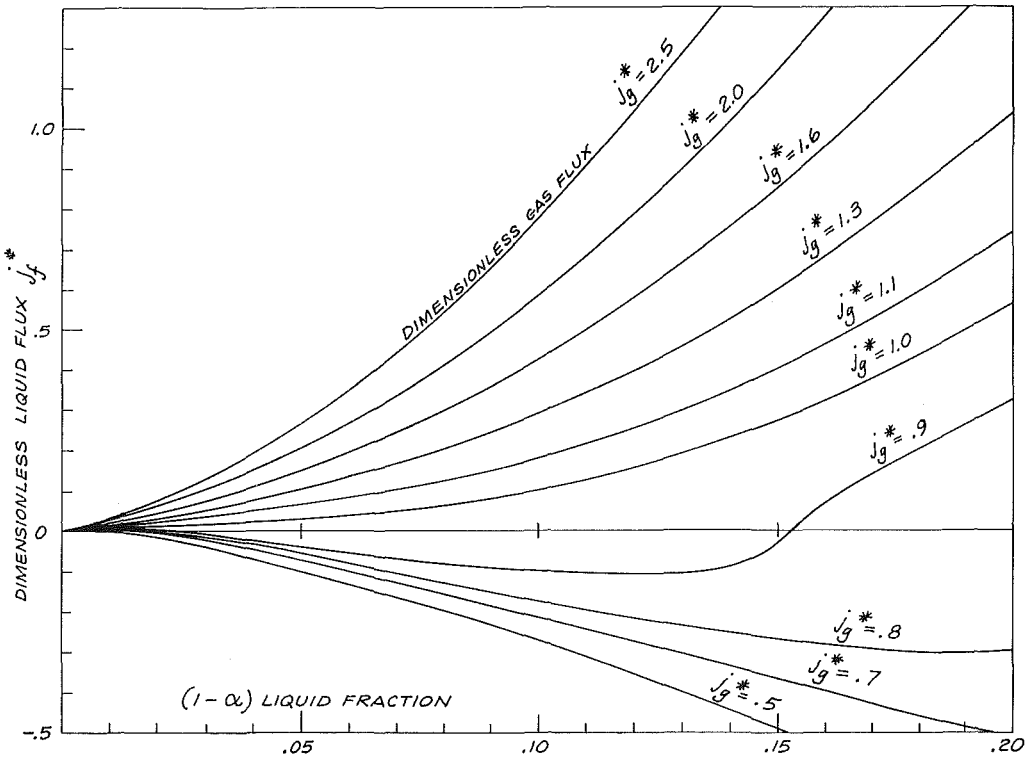

Fig. 5 j_f^* versus $(1 - \alpha)$ for various values of j_g^* for a turbulent film

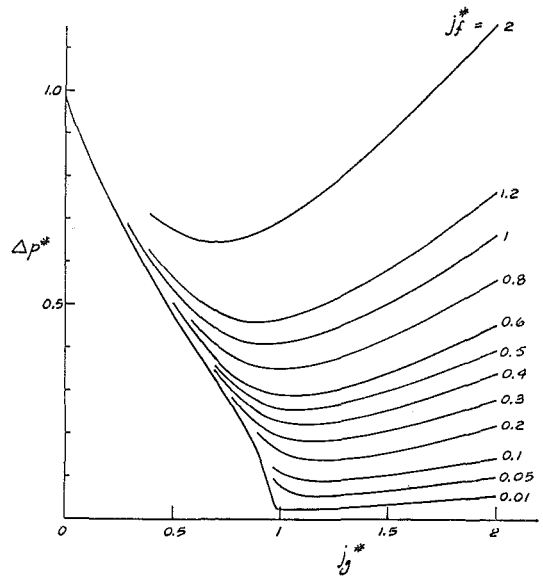

Fig. 6 Dimensionless pressure drop ΔP^* versus dimensionless gas flux j_g^*, for various values of j_f^* (turbulent film)

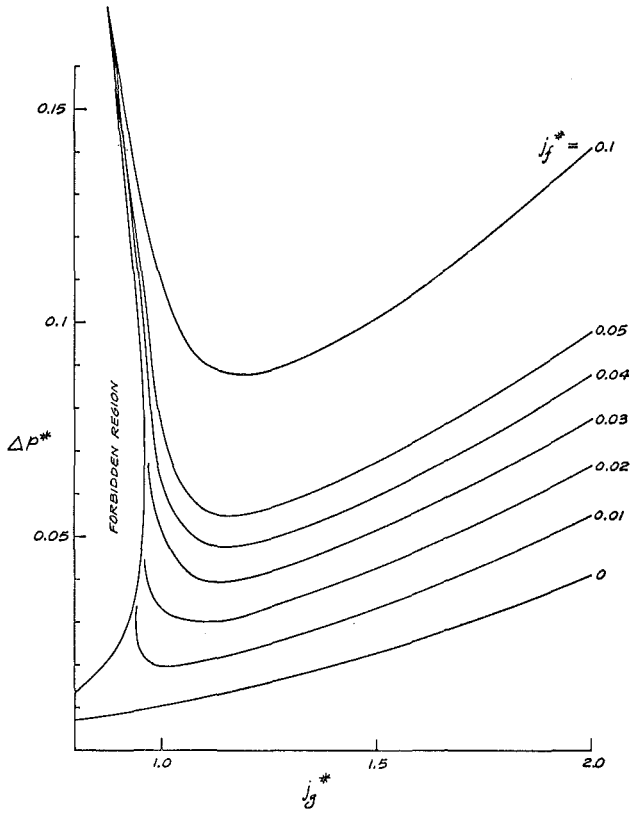

Fig. 7 Enlargement of Fig. 6 for low values of j_f^*

$$j_g^* = \frac{j_g \rho_g^{1/2}}{[gD(\rho_f - \rho_g)]^{1/2}} \tag{24}$$

$$j_f^* = \frac{j_f \rho_f^{1/2}}{[gD(\rho_f - \rho_g)]^{1/2}} \tag{25}$$

$$j_f^{1*} = \frac{32 j_f \mu_f}{D^2 g(\rho_f - \rho_g)} \tag{26}$$

In terms of these parameters, equations (19), (21), and (22) become

$$\Delta P^* = 10^{-2} j_g^{*2} \frac{1 + 75(1 - \alpha)}{\alpha^{5/2}} \tag{27}$$

$$\text{Turbulent } \Delta P^* = (1 - \alpha) + 10^{-2} \frac{j_f^* |j_f^*|}{(1 - \alpha)^2} \tag{28}$$

$$\text{Laminar } \Delta P^* = \frac{j_f^{1*}}{(1 - \alpha)^2} + (0.684)(1 - \alpha) \tag{29}$$

If the turbulent flow solution could be obtained by a differential analysis of the film, the first term on the right-hand side of equation (28) would presumably be slightly modified.

The liquid film Reynolds number is

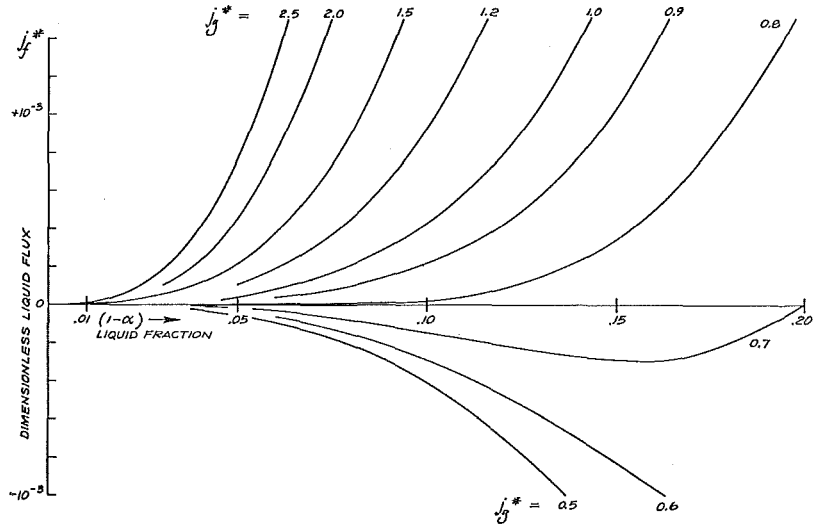

Fig. 8 j_f^* versus $(1 - \alpha)$ for various values of j_g^* (laminar film)

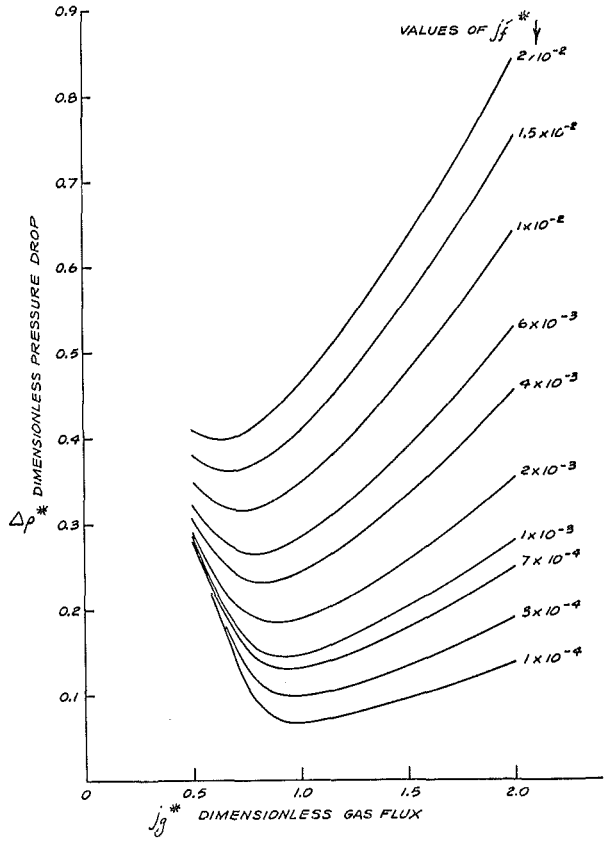

Fig. 9 ΔP^* versus j_g^* for various values of $j_f'^*$ (laminar film)

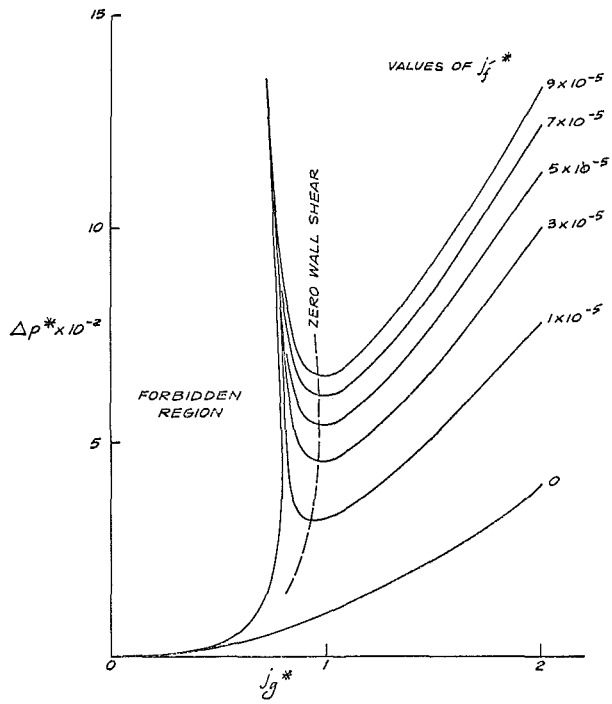

Fig. 10 Detail of Fig. 9 at low values of $j_f'^*$

$$\mathrm{Re}_f = \frac{j_f \rho_f D}{\mu_f} \tag{30}$$

A further useful dimensionless quantity is

$$N_f = \frac{D^{3/2}\rho_f^{1/2} g^{1/2}}{\mu_f} (\rho_f - \rho_g)^{1/2} \tag{31}$$

It is readily found that

$$\mathrm{Re}_f = j_f^* N_f \tag{32}$$

and

$$j_f{}^{1*} = 32 j_f^*/N_f \tag{33}$$

Equations (27)–(29) were solved on the Dartmouth GE 235 computer for numerous values of the parameters by Andrew Porteous. The major results are plotted in Figs. 5 through 10. Fig. 11 gives a rapid way of predicting both ΔP^* and $(1 - \alpha)$ in terms of the dimensionless flow rates and is close to a similar empirical correlation scheme presented by Turner [6]. In Fig. 10, the line of zero wall shear is derived by equating the pressure gradient and the gravitational forces to obtain

$$\Delta P^* = (1 - \alpha) \tag{34}$$

Using this result in equation (29), we get

$$\frac{j_f{}^{1*}}{(1 - \alpha)^2} = 0.316(1 - \alpha) \tag{35}$$

The zero wall shear line is seen almost to coincide with the locus of the pressure-drop minima.

The pressure-drop minimum, at a given liquid flow rate, can be obtained from equations (28) and (29) by differentiation. For laminar flow, we have

$$\frac{d\Delta P^*}{d(1 - \alpha)} = \frac{-2 j_f{}^{1*}}{(1 - \alpha)^3} + 0.684 \tag{36}$$

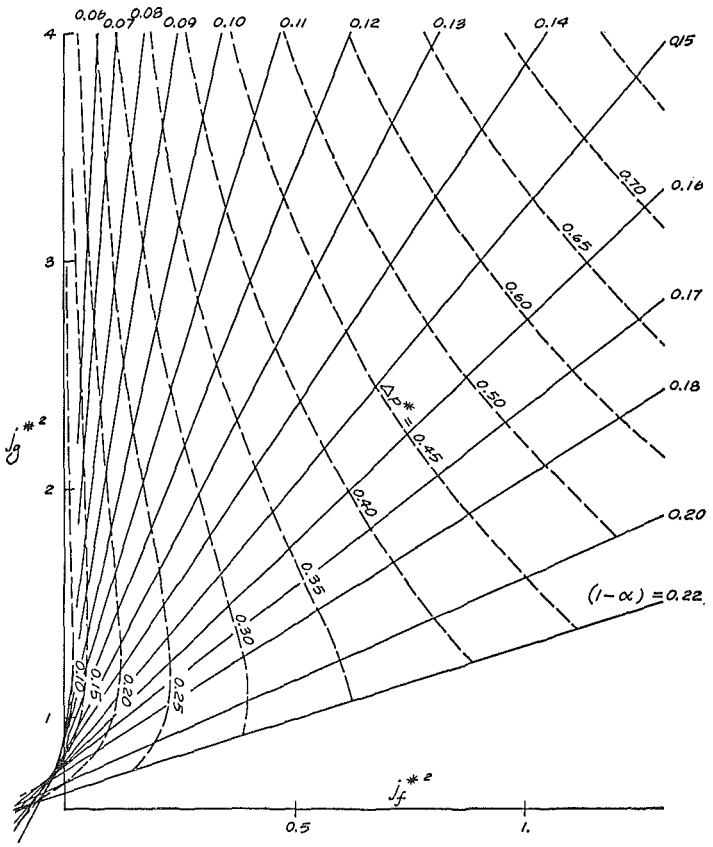

Fig. 11 ΔP^* and $(1 - \alpha)$ as functions of j_g^{*2} and j_f^{*2} (turbulent film)

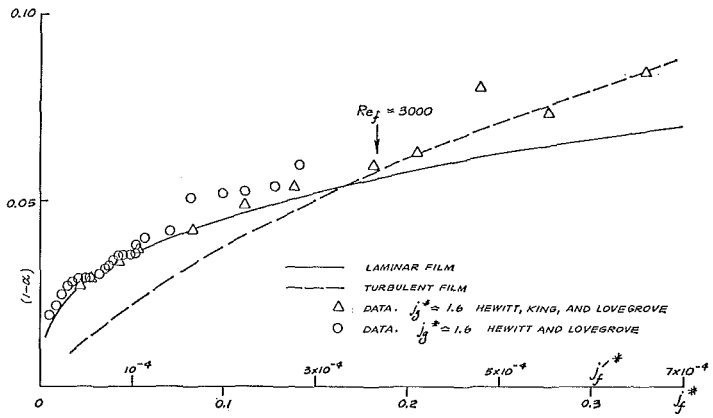

Fig. 12 Comparison between present theory and data of Hewitt, King, and Lovegrove (1.25-in. dia, air-water ≈ 15 psia)

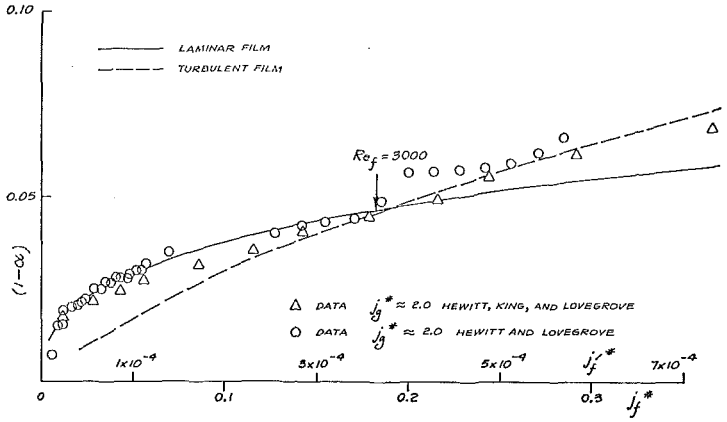

Fig. 13 Comparison between present theory and data of Hewitt, King, and Lovegrove (1.25-in. dia, air-water ≈ 15 psia)

The minimum occurs when

$$j_f{}^{1*} = 0.342(1 - \alpha)^3 \tag{37}$$

or

$$(1 - \alpha) = 1.43 j_f{}^{1*1/3} \tag{38}$$

The corresponding value of the pressure drop is

$$\Delta P_{\min}{}^* = 1.47 j_f{}^{1*1/3} \tag{39}$$

Since equations (38) and (39) are almost exactly compatible with equation (34), and equations (35) and (37) are much the same, the pressure-drop minimum is indeed very close to the point of zero wall shear.

For turbulent flow, a similar treatment of equation (28) gives, at the minimum pressure drop

$$(1 - \alpha) = 0.272 j_f{}^{*2/3} \tag{40}$$

$$\Delta P_{\min}{}^* = 0.41 j_f{}^{*2/3} \tag{41}$$

In general, for a friction factor of f_w, instead of the assumed value of 0.005, the results are

$$(1 - \alpha) = 0.272 \left(\frac{f_w}{0.005}\right)^{1/3} j_f{}^{*2/3} \tag{42}$$

$$\Delta P_{\min}{}^* = 0.41 \left(\frac{f_w}{0.005}\right)^{1/3} j_f{}^{*2/3} \tag{43}$$

Thus an increase in wall friction factor increases the minimum pressure drop.

Several important qualitative aspects of the graphs deserve attention. First, it is evident from Fig. 5 that the character of the flow changes quite dramatically when $j_g{}^*$ falls below about unity. No downflow is possible unless $j_g{}^*$ is less than 0.95, and a slight reduction below this value requires high liquid fractions before upflow can occur. (There is actually a slight region of upflow near the origin which only allows $j_f{}^*$ values below 0.01.) Practically, a value of $j_g{}^* = 0.9$ corresponds to a situation in which thin liquid films flow downward while thick ones flow upward. A net upflow of liquid then usually occurs as a result of "waves" of thick film riding over a smoother and thinner falling film. With values of $j_g{}^*$ below 0.9, these thick films are usually sufficient to bridge the pipe temporarily and bring about a transition to slug flow. This conclusion is consistent with the empirical conclusion of Wallis [7] that the onset of annular upflow at low liquid rates occurs between $j_g{}^* = 0.8$ and 0.9.

In the case of laminar flow, Fig. 8, the picture is much the same with the transition occurring at $j_g{}^* = 0.8$.

The pressure-drop graphs for low liquid rates, Figs. 7 and 10, display the same effects in a different way. Below a gas rate in the range $0.8 < j_g{}^* < 1$, the pressure drop increases immensely and there is a "forbidden region" in which no solutions can be obtained. Since one is often dealing in practice with systems in which the pressure drop is controlled by the external characteristics, this forbidden region can be very significant since an attempt to operate in it results in either a new flow regime or an unstable situation in which a large change in the operating conditions occurs. Moreover, at a gas flux which crosses this forbidden region at low liquid flow rates, there are three possible solutions to the pressure drop for a given liquid rate. Rather small fluctuations in any one of the parameters can then lead to a jump from the low-pressure drop to the high-pressure drop value.

The pressure-drop minimum at a constant liquid rate is also of significance for determining the stability of a system in which the pressure drop and liquid rate are controlled. If the gas rate is allowed to fall below the value corresponding to the minimum pressure drop, it will continue to fall until the pipe fills with liquid and becomes flooded.

In general, the first-order stability of any system will be determined by the interaction between these pressure-drop characteristics and the properties of the device to which it is connected.

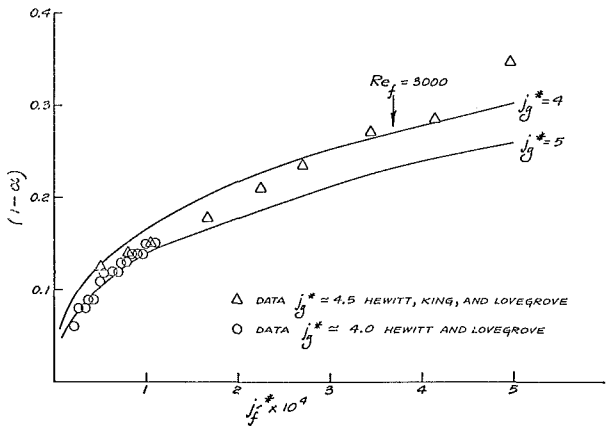

Fig. 14 Comparison between laminar film theory and data of Hewitt, King, and Lovegrove, for high values of $j_g{}^*$ (1.25-in. dia, air-water, 15–20 psia)

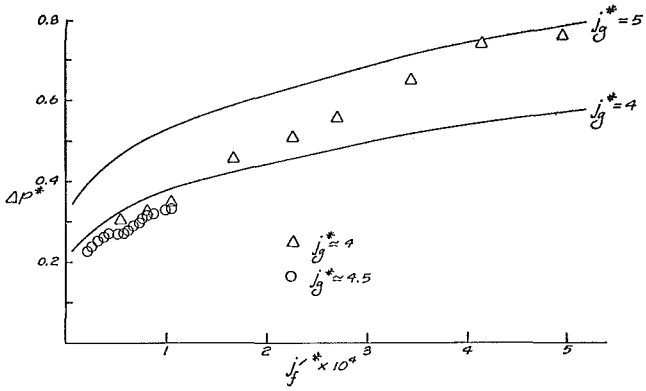

Fig. 15 Pressure-drop data corresponding to conditions of Fig. 14 compared with theoretical values

Fig. 11 also shows that the maximum liquid rate at a given pressure drop occurs at a value of $j_g{}^*$ equal to about 1.1 (for $\Delta P^* < 0.3$).

Comparison Between Theory and Data

In order to establish the validity of the theory over a range of conditions, it has been compared with a large variety of data from several sources.

Figs. 12–14 show liquid fraction predictions compared with data of Hewitt, King, and Lovegrove [8], and of Hewitt and Lovegrove [9]. The data are seen to be close to the laminar film prediction up to a value of the liquid Reynolds number of about 3000, and to follow the turbulent film line thereafter. This value of the "transition Reynolds number" is probably not universal, since one would expect some dependence on the gas characteristics and perhaps also on the surface tension. Moreover, close to the flow reversal point at $j_g{}^* \approx 1$, an agitated and plainly turbulent film can exist even when the value of j_f (and Re_f) is equal to zero.

One cause of deviation from the theory at the higher liquid rates is the significant proportion of the liquid flow which is entrained in the form of droplets (as reported by Gill and Hewitt [10]). It would seem that a more sophisticated theory which takes account of this entrainment would lead to greater accuracy. However, the simple theory still provides a reasonable first approximation.

Fig. 15 also shows a reasonable prediction of the pressure drop for the conditions in Fig. 14.

Fig. 16 shows a comparison with the data of Bennett and Thornton [11] for low liquid rates and small amounts of entrainment.

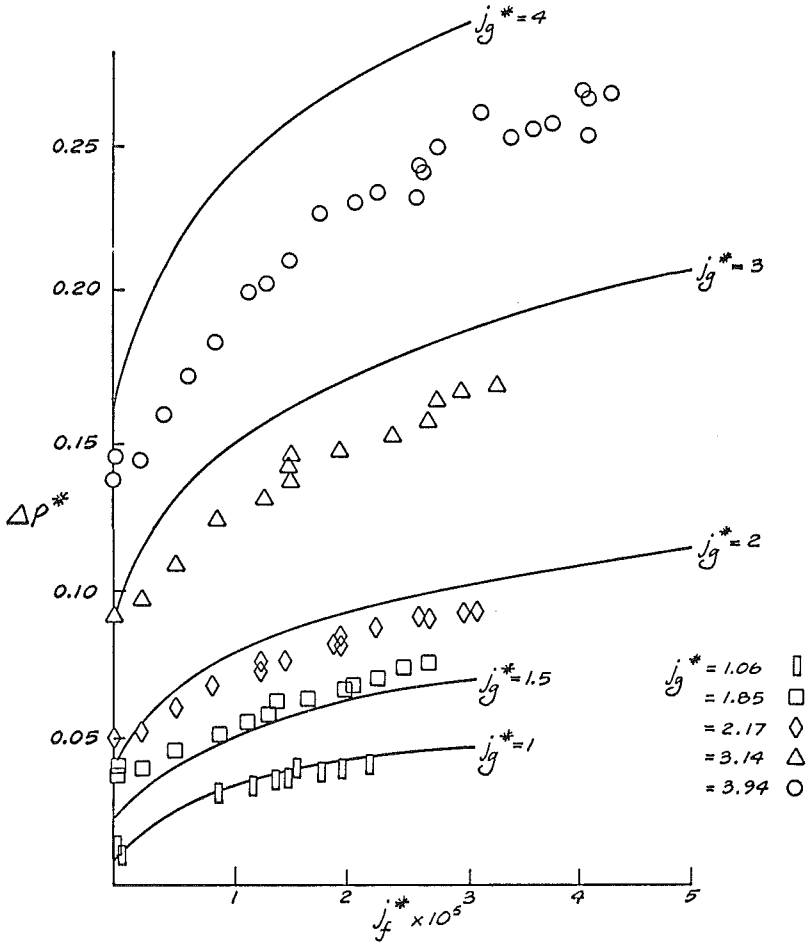

Fig. 16 Comparison between data of Bennett and Thornton and the present theory (laminar film) 1.36-in. dia, air-water, "atmospheric" pressure

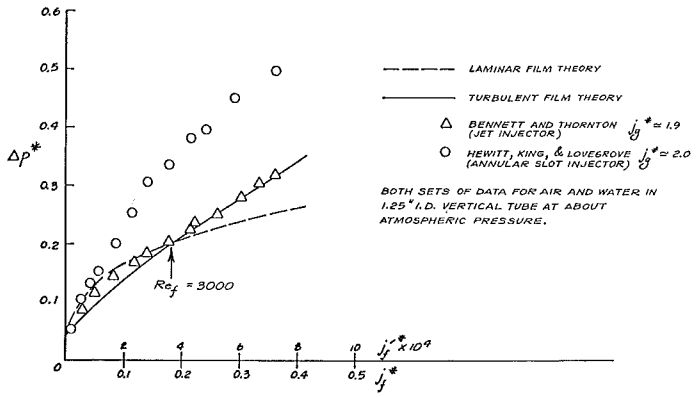

Fig. 17 Comparison between theory and data of two different investigations at same flow rates but using differing injection techniques

Fig. 17 shows how the pressure drop can vary significantly as a function of the method of injection of the liquid into the pipe. These "entrance effects," which are mostly due to the distance which is taken to establish the entrained droplet flow, lead to typical variations of the order of 50 percent in pressure drop and are not accounted for by the present theory.

Fig. 18 shows the data of Hewitt, Lacey, and Nicholls [12] in the region of the pressure-drop minimum. The data points at the lowest gas flow rates shown correspond to the onset of flow reversal and are close to the boundary of the forbidden region in Fig. 10.

Fig. 19 shows the variation of airflow rate at the pressure-drop minimum for low liquid rates as a function of pipe diameter. The data are pretty well located on a line of constant j_g^*, except for the data of Willis [13]. It will be seen later that Willis' data display further anomalies which are mainly resolved if the gas flow rate is modified by the factor 1.5, as indicated by Fig. 19.

Figs. 20 and 21 compare the present laminar and turbulent film theories with the pressure-drop and void fraction correlations of Turner [6]. In general, the laminar theory is close to the correlation at low liquid rates and the turbulent theory is more appropriate at higher values.

Fig. 22 compares the theory with the data of Anderson and Mantzouranis [14] in a rather small pipe. The laminar film theory gives good predictions for liquid Reynolds numbers below 3000.

Fig. 23 shows Willis' data. In order to obtain a good comparison, it was necessary to change the scale of the gas flow rate as indicated in Fig. 19. Furthermore, the data at high liquid rates followed, very precisely, curves corresponding to rather different

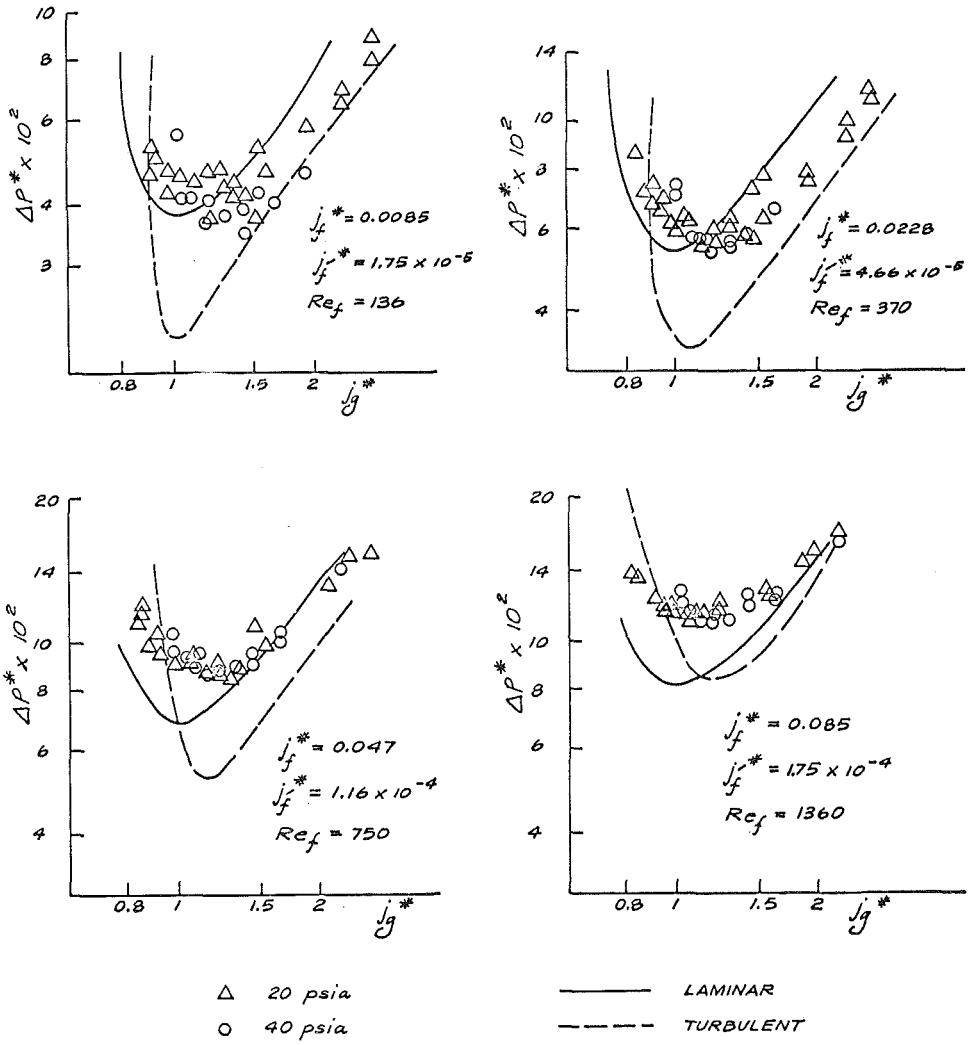

Fig. 18 Data of Hewitt, Lacey, and Nicholls, air and water in 1.25-in. pipe close to point of minimum pressure gradient

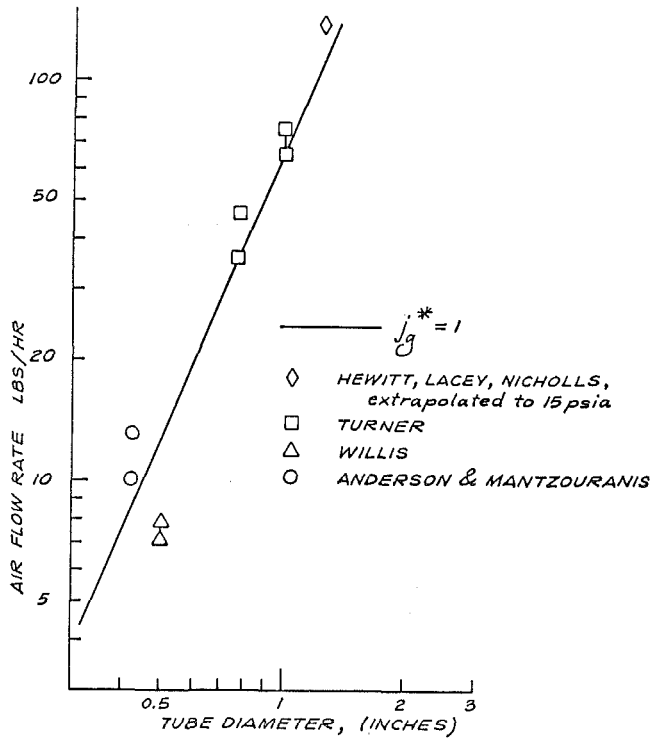

Fig. 19 Location of minimum pressure drop at low liquid rates ($\Delta P^* \approx 0.1$) as a function of tube dia; air-water systems at 15 psia

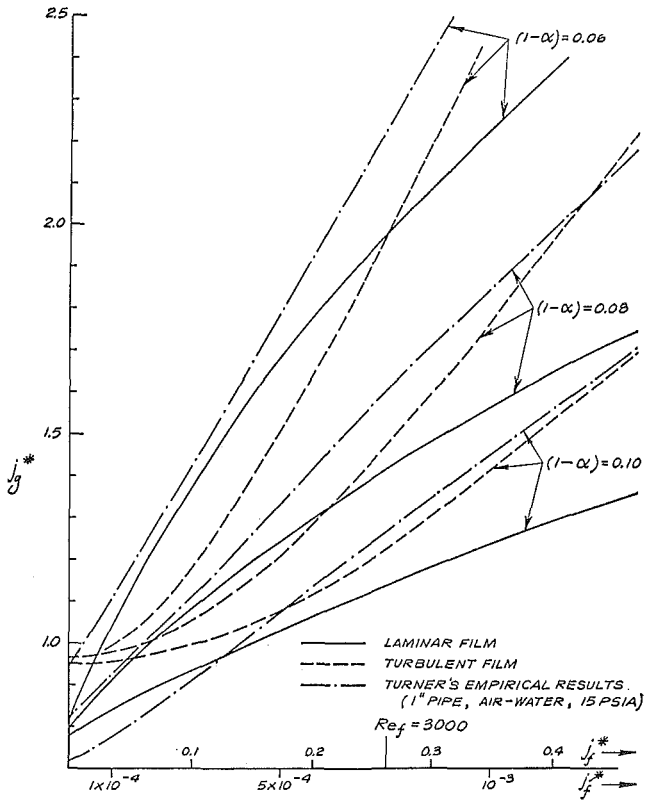

Fig. 20 Comparison with Turner's results

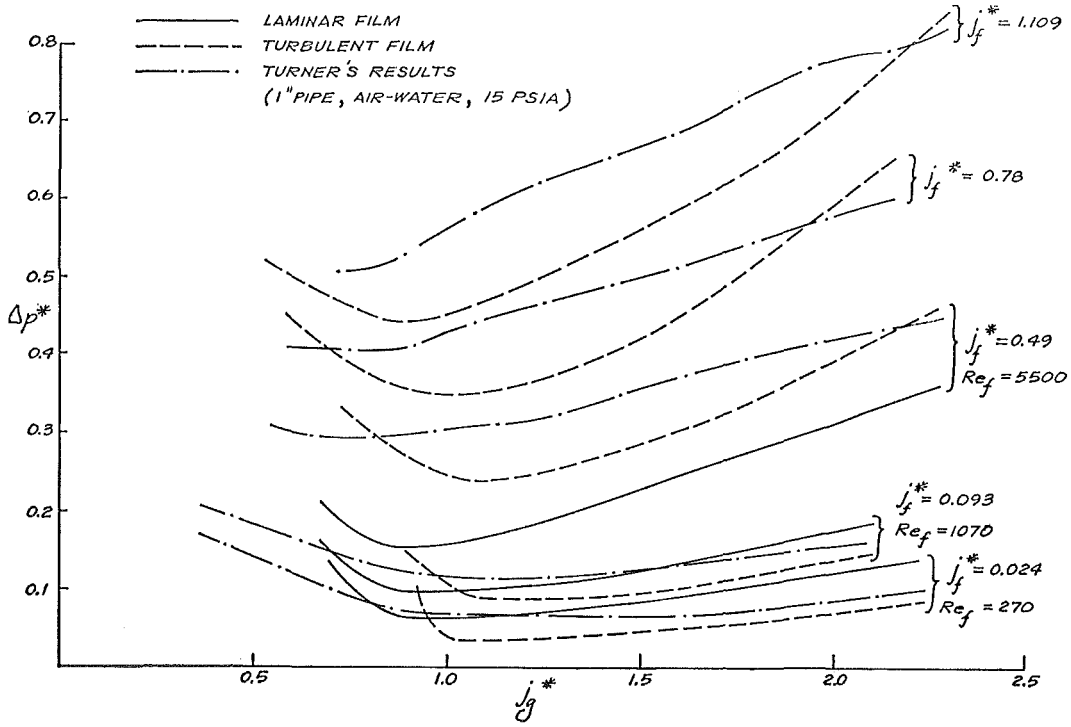

Fig. 21 Comparison with Turner's results

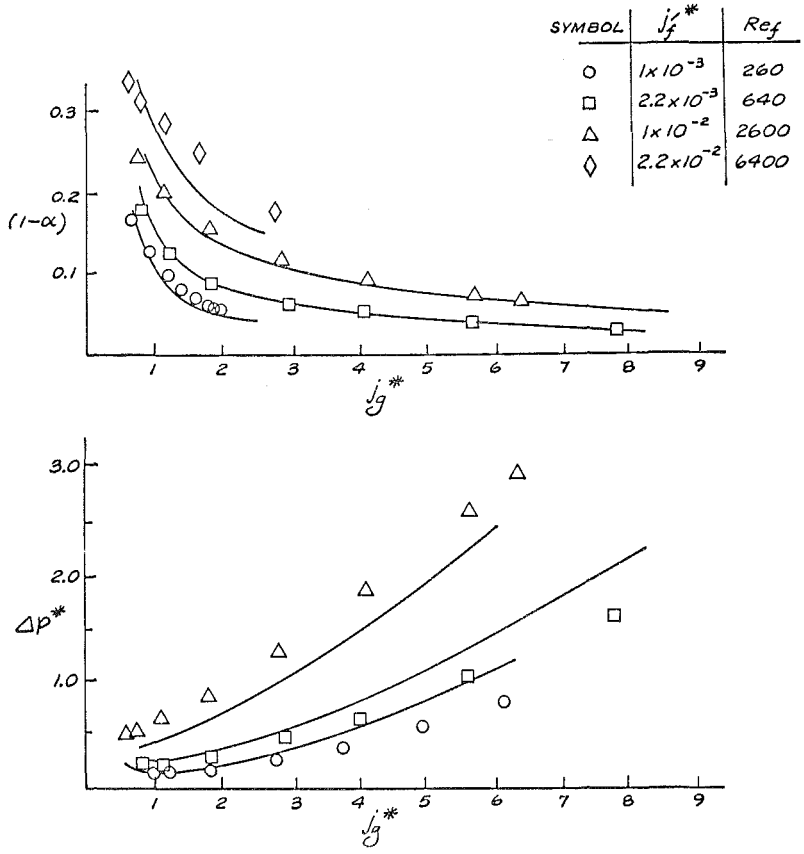

Fig. 22 Comparison between present theory for a laminar film, and data of Anderson and Mantzouranis (0.427-in. dia, air-water 15 psia)

liquid rates. Perhaps, the method of injection used by Willis led to a rather high percentage of entrainment of the liquid flow.

Fig. 24 shows a reasonable comparison with CISE data at high pressure for an argon-water system [15].

Comparison With Levy's Theory

Levy [16] has recently presented a theory of annular flow which is much more sophisticated than the present analysis, but eventually leads to a method for representing the interfacial shear stress. Levy also distinguishes between the conditions $\Delta P^* \lesssim 1$, which determine the curvature of the velocity distribution in the liquid film.

For $\Delta P^* > 1$, Levy plots a function F^1 which, in the present notation with negligible entrainment, is

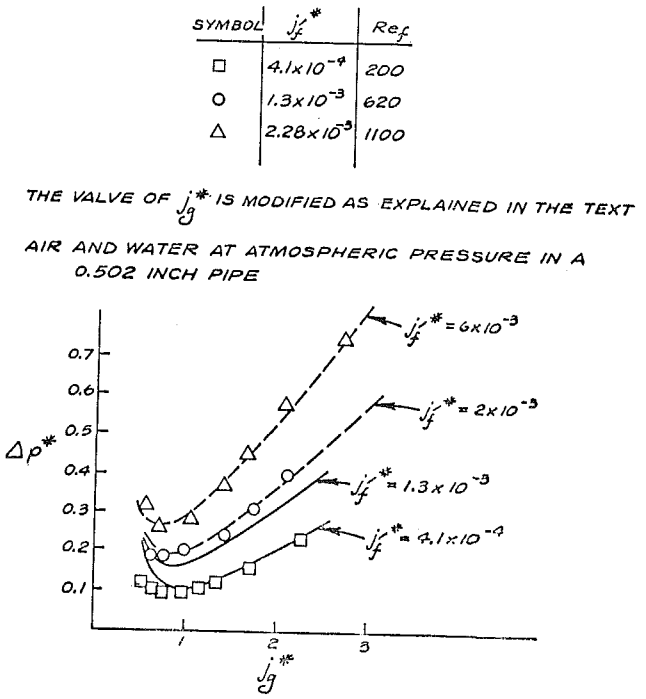

Fig. 23 Pressure-drop data of Willis compared with present theory

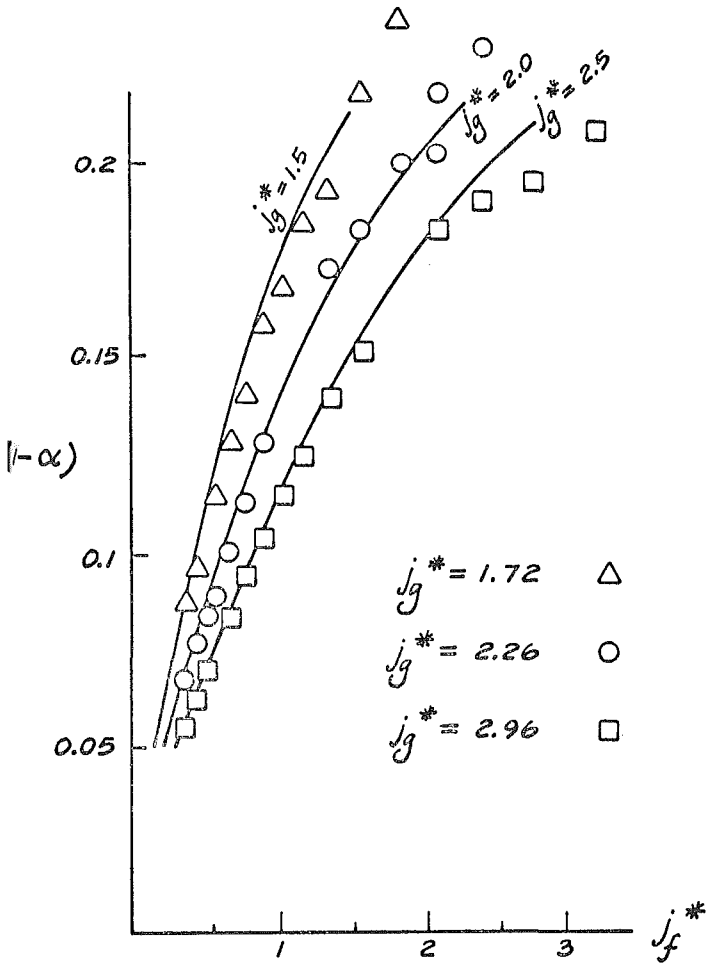

Fig. 24 Comparison between present theory for a turbulent film and CISE data for argon-water mixtures at 310 psia in a vertical 2.5-cm-ID tube

$$F^1 = \left[\frac{\tau_i}{V_g(V_g - V_f)(\rho_f - \rho_g)}\right]^{1/2} R \tag{44}$$

R is an empirical function of density ratio shown in Fig. 25 and can be represented quite well by the equation

$$R = \frac{1}{2}\sqrt{\frac{\rho_f}{\rho_g}} \tag{45}$$

Making the following approximations, which are consistent with the level of sophistication of the present theory

$$\rho_f \gg \rho_g$$

$$V_g \gg V_f$$

Equations (44) and (45) can be combined to give

$$F^1 \approx \left[\frac{\tau_i}{4\rho_g V_g^2}\right]^{1/2} \tag{46}$$

Whence, using equation (3),

$$F^1 \approx \left[\frac{f_i}{8}\right]^{1/2} \tag{47}$$

Levy goes on to plot F^1 versus the ratio of the average film thickness to the pipe radius. In view of equation (47), this is just what was done in Fig. 3 of this paper. We can, therefore, compare the two theories directly by plotting equation (16) on Levy's graphs. The results shown in Figs. 26, 27, and 28 are pleasantly favorable. Large differences occur above a value of $2\delta/D = 0.15$, but this is almost certainly in the region of slug-annular flow which usually occurs for $(1 - \alpha) > 0.2$ [or $2\delta/D \gtrsim 0.1$].

For $\Delta P^* < 1$, Levy introduces a correction factor $(\Delta P^*)^{1/3}$ which multiplies the function F^1. This factor is never less than $1/2$, and is closer to unity for most of the CISE data considered by Levy. However, it may well be that the addition of the parameter ΔP^* in Fig. 3 could lead to an improvement in accuracy.

It can be concluded that the present theory is a reasonable approximation to Levy's; it is simpler, but is, perhaps, less accurate.

Comparison With Results of Solov'ev, Preobrazhenskii, and Semenov. In reference [17], it was found that a plot of $\Delta P^*/\Delta P_{\text{min}}{}^*$ versus $j_g{}^*/j_{g_{\text{min}}}{}^*$ for a laminar film gave a unique curve for all liquid rates. Fig. 29 shows the present theory plotted in this way as well as the empirical curve from reference [17]. Agreement is surprising considering that $j_f{}'^*$ is varied over three orders of magnitude. Since $j_{g_{\text{min}}}{}^*$ is approximately constant and is close to unity, the abscissa has been chosen as $j_g{}^*$, although dividing by $j_{g_{\text{min}}}{}^*$ gives a slightly better comparison.

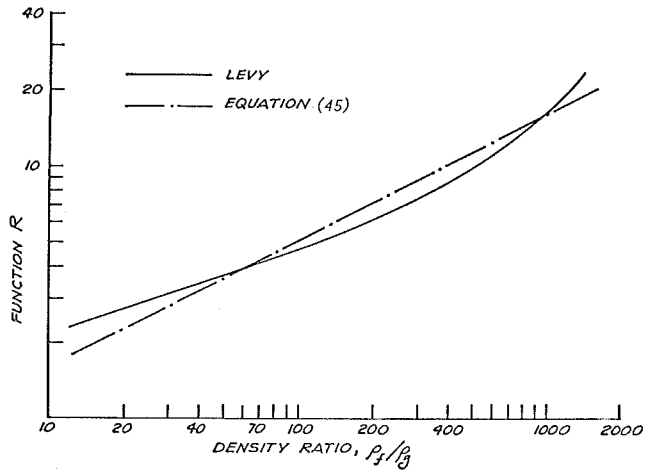

Fig. 25 Function R of density ratio ρ_f/ρ_g

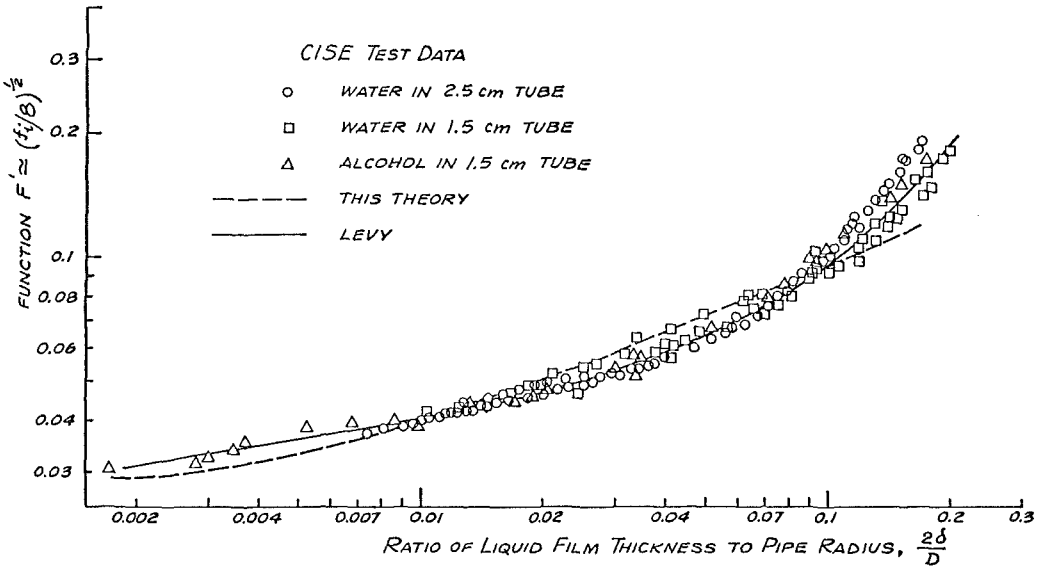

Fig. 26 Comparison between present theory and Levy's correlation of CISE data (vertical flow)

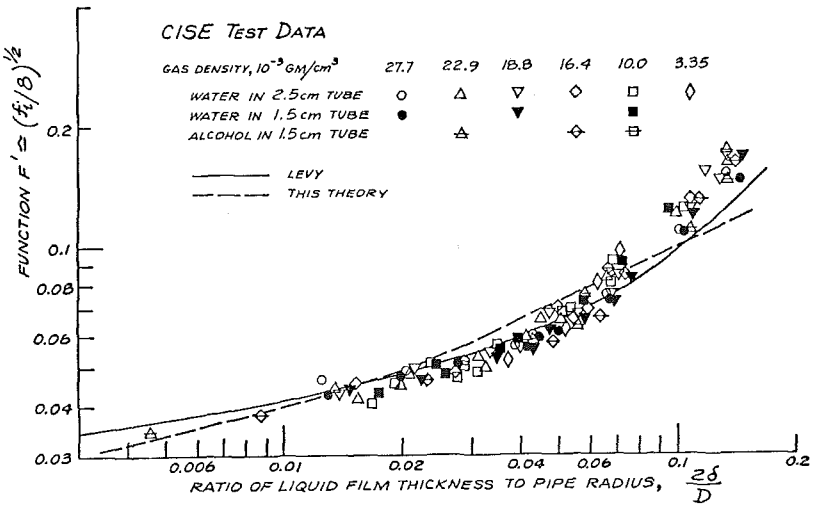

Fig. 27 Further comparisons with Levy's work

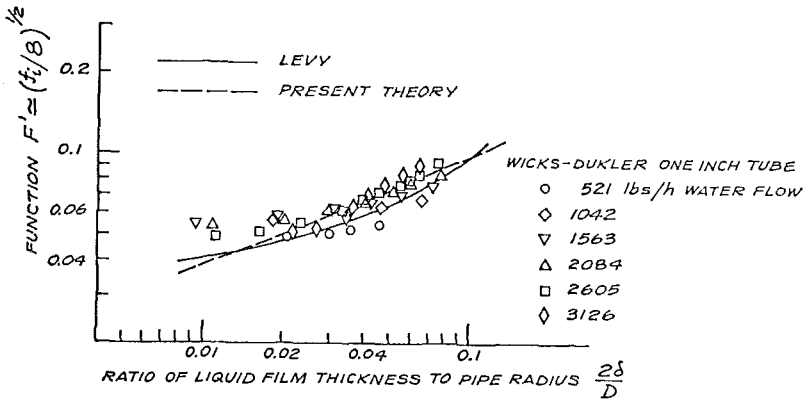

Fig. 28 Comparison with data for horizontal flow

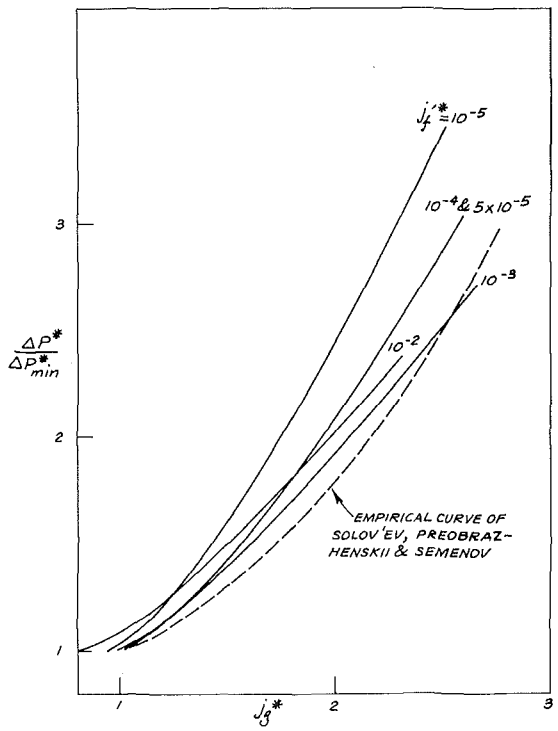

Fig. 29 Comparison between laminar film theory and results of reference [17]

Representation in Terms of "Superficial" Gas Friction Factor. An alternative interpretation of equation (19) is that the pressure drop can be calculated by considering that the gas alone flows in a pipe of diameter D with a superficial friction factor, f_{sg}, of

$$f_{sg} = 0.005 \frac{[1 + 75(1 - \alpha)]}{\alpha^{5/2}} \tag{48}$$

A simpler equation, which gives much the same result, is

$$f_{sg} = 0.005[1 + 90(1 - \alpha)] \tag{49}$$

and is easy to remember by the rule-of-thumb that a liquid fraction of one tenth increases the pressure drop by a factor of 10.

Horizontal Flow, Comparison With Martinelli's Correlation. In horizontal flow the gravitational terms disappear from equations (28) and (29), and we have, for the liquid

$$\Delta P^* = 10^{-2} \frac{j_f'^{*2}}{(1 - \alpha)^2} \quad \text{(turbulent)} \tag{50}$$

$$\Delta P^* = \frac{j_f'^*}{(1 - \alpha)^2} \quad \text{(laminar)} \tag{51}$$

Since it has already been assumed that the turbulent friction factor is 0.005 for single-phase flow, each of these equations is equivalent to the following expression for Martinelli's parameter, ϕ_f

$$\phi_f = \frac{1}{(1 - \alpha)} \tag{52}$$

Combining equation (52) with (20), we get

$$X = \frac{\phi_g}{\phi_f} = \frac{(1 - \alpha)[1 + 75(1 - \alpha)]}{\alpha^{5/2}} \tag{53}$$

for either laminar or turbulent flow of the liquid. This equation is compared with Martinelli's correlation and data in Fig. 30.

Discussion

A very simple correlation of the interfacial friction factor in annular flow as a function of the liquid fraction, or ratio of film thickness to pipe diameter, has been shown to give good comparison with a wide variety of data, as well as with several earlier theories and correlations. The resulting theory is suitable for the prediction of liquid fraction, pressure drop, and stability limits of annular gas-liquid and vapor-liquid flows.

The accuracy of this theory can be extended by introducing further parameters (involving surface tension, gas and liquid viscosities, ΔP^*, density ratio, compressibility, etc.) into the correlation scheme shown in Fig. 3. Furthermore, the friction factors can also be correlated against further parameters (such as Reynolds numbers) instead of being assumed to be always 0.005 in turbulent flow. If the level of liquid entrainment is known, the theory can be adapted to treat the core as a homogeneous mixture, while the remaining liquid flows in the film. These topics will be taken up in Part 2 of this paper [18].

The major contribution of this work is the establishment of a simple, but remarkably effective theory, which is readily improved in accuracy by introducing greater levels of sophistication. For many engineering problems added complexity is not worth while and the simple theory is quite adequate.

Acknowledgments

Partial support for this study was provided by Scott Paper Company through a contract with Creare, Inc., Hanover, N. H. The data in Fig. 3 and the approximately linear relationship between interfacial friction factor and film thickness were first brought to the author's attention by P. J. Kroon, who developed a successful theory of annular-mist flow for a particular applica-

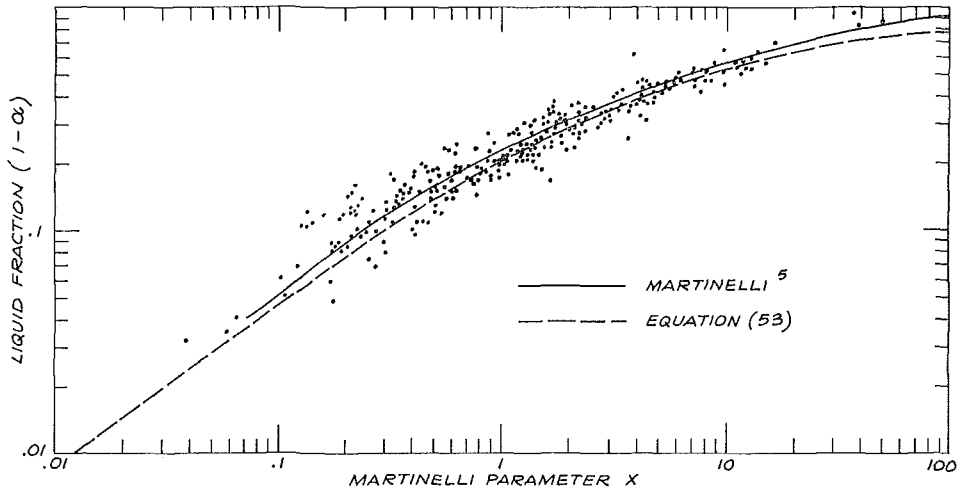

Fig. 30 Comparison of liquid fraction predicted by equation (53) with empirical results of Martinelli [5]

tion. This paper was developed from an unpublished presentation by the author at a symposium organized by the American Institute of Chemical Engineers at Tampa, Fla., May 1968.

References

1 Bergelin, O. P., et al., "Cocurrent Gas-Liquid Flow," Heat Transfer and Fluid Mechanics Institute, Berkeley, Calif., 1949.

2 Kroon, P. J., Personal communication, 1967.

3 Nikuradse, J., "Strömungsgesetze in rauhen Rohren," *Forschungsheft*, 1933, p. 361.

4 Moody, L. F., "Friction Factors for Pipe Flow," TRANS. ASME, Vol. 66, 1944, p. 671.

5 Lockhart, R. W., and Martinelli, R. C., "Proposed Correlation of Data for Isothermal Two-Phase, Two-Component Flow in Pipes," *Chemical Engineering Progress*, Vol. 45, 1944, p. 39.

6 Turner, J. M., PhD thesis, Dartmouth College, 1966.

7 Wallis, G. B., "The Transition From Flooding to Upward Cocurrent Annular Flow in a Vertical Pipe," AEEW-R142, UKAEA, 1962.

8 Hewitt, G. F., King, I., and Lovegrove, P. C., "Holdup and Pressure-Drop Measurements in the Two-Phase Annular Flow of Air-Water Mixtures," AERE-R3764, UKAEA, 1961.

9 Hewitt, G. F., and Lovegrove, P. C., "Comparative Film Thickness and Holdup Measurements in Vertical Annular Flow," AERE-M1203, UKAEA, 1963.

10 Gill, L. E., and Hewitt, G. F., "Further Data on the Upward Annular Flow of Air-Water Mixtures," AERE-R3935, UKAEA 1962.

11 Bennett, J. A. R., and Thornton, J. D., "Pressure-Drop Data for the Vertical Flow of Air-Water Mixtures in the Climbing-Film and Liquid-Dispersed Regions," AERE-R3195, UKAEA, 1965.

12 Hewitt, G. F., Lacey, P. M. C., and Nicholls, B., "Transitions in Film Flow in a Vertical Tube," AERE-R4614, UKAEA, 1965.

13 Willis, J. J., "Upward Annular Two-Phase Air/Water Flow in Vertical Tubes," *Chemical Engineering Science*, Vol. 20, 1965, pp. 895–902.

14 Anderson, G. H., and Mantzouranis, B. G., "Two-Phase (Gas-Liquid) Flow Phenomena—1," *Chemical Engineering Science*, Vol. 12, 1960, pp. 109–126.

15 Collier, J. G., and Hewitt, G. F., "Film Thickness Measurements," AERE-R4684, UKAEA, 1964.

16 Levy, S., "Prediction of Two-Phase Annular Flow With Liquid Entrainment," *International Journal of Heat and Mass Transfer*, Vol. 9, 1966, pp. 171–188.

17 Solov'ev, A. V., Preobrazhenskii, E. I., and Semenov, P. A., "Hydraulic Resistance in Two-Phase Flow," *International Chemical Engineering*, Vol. 7, No. 1, 1967, pp. 59–64.

18 Wallis, G. B., "Annular Two-Phase Flow—Part II: Additional Effects," ASME Paper No. 69-FE-46, 1969.